

# Electrical Characterization of Benzocyclobutene Polymers for Electric Micromachines

Alireza Modafe, *Student Member, IEEE*, Nima Ghalichechian, *Student Member, IEEE*, Benjamin Kleber, and Reza Ghodssi, *Member, IEEE*

**Abstract**—An approach using interdigitated capacitors for electrical characterization of CYCLOTENE, a spin-on low- $k$  benzocyclobutene (BCB)-based polymer is introduced and the effect of moisture uptake is investigated. The dielectric constant of CYCLOTENE is extracted from capacitance measurements with a systematic error less than 0.1%, giving an average value of 2.49 with a standard deviation of 1.5%. The dielectric constant increases by 1.2% after a humidity stress of 85% RH at 85°C. The  $I$ - $V$  characteristics of CYCLOTENE show a dependency of breakdown strength and leakage current on the geometrical dimensions of the device under test. A breakdown strength of 225 V/ $\mu$ m and 320 V/ $\mu$ m for 2- $\mu$ m and 3- $\mu$ m finger spacing, respectively, and a leakage current of a few to tens of pA are measured. The  $I$ - $V$  characteristics degrade drastically after the humidity stress, showing a breakdown strength of 100 V/ $\mu$ m and 180 V/ $\mu$ m for 2- $\mu$ m and 3- $\mu$ m finger spacing, respectively, and a maximum increase in the leakage current as large as one order of magnitude. The maximum performance and long-term reliability of an electric micromachine are adversely affected by the degradation of the breakdown voltage and the leakage current after moisture absorption. It is expected, however, that the electrical efficiency is improved using BCB-based polymers with negligible dependency on moisture absorption.

**Index Terms**—Benzocyclobutene (BCB), CYCLOTENE, dielectric insulating layer, electrical characterization, electric micromachines.

## I. INTRODUCTION

MICROELECTROMECHANICAL systems (MEMS) and devices for power conversion, known as Power MEMS [1], have been attractive since the early days of MEMS. It is desirable to integrate electric motors and power generators, mechanical pumps and valves, chemical reactors and combustors, and even engines on a single chip to achieve high power density for applications with tight power requirements. In light of scientific and technological advances in microfabrication in the last two decades, Power MEMS is now becoming a promising technology in variety of microsystem applications such as microscale electrical power generation [2], micropropulsion [3], microrobotics and micromechatronics [4]. However, realization of high-power, efficient, reliable Power MEMS requires further research.

Manuscript received December 7, 2003; revised February 3, 2004. This work was supported by the National Science Foundation under Grant ECS-0224361, the Minta Martin Program, and the Small Smart Systems Center at the University of Maryland.

The authors are with the Department of Electrical and Computer Engineering and the Institute for Systems Research, University of Maryland, College Park, MD 20742 USA (e-mail: ghodssi@eng.umd.edu).

Digital Object Identifier 10.1109/TDMR.2004.830289

The very early Power MEMS devices were side-drive, variable-capacitance micromotors fabricated with polysilicon surface micromachining technology [5]–[9]. In these devices, the electrical insulating layer mainly consisted of 1–2  $\mu$ m films of thermal silicon dioxide or LPCVD silicon nitride, exhibiting large stress, high dielectric constant, and reliability issues. The development of the first micromotors [6] was a successful demonstration of power conversion on a microscale, however, the level of power, efficiency and reliability achieved is not satisfactory for the power demands in microsystems.

The demand for higher power and efficiency in Power MEMS has pushed the required thickness of the electrical insulating layer to tens of micrometers to meet the high voltage and energy loss requirements. It has also initiated many research activities on the use of tetraethylorthosilicate (TEOS)-based and silane-based plasma-enhanced chemical-vapor-deposited (PECVD) silicon dioxide to develop crack-free, low-stress, thick insulating layers [10]–[14]. The major issues in the development of thick PECVD oxide films are wafer bow and cracks developed during cure processes as a result of excessive residual stress. Thick buried oxide in silicon (TBOS) [10] was developed as an integrated fabrication technology to reduce the wafer bow and film cracks in the electrical stator of a high-voltage micromotor. However, the reduced wafer bow was still large and the crack-free film thickness could not be beyond 15  $\mu$ m. Furthermore, there are still many challenging issues facing the use of PECVD-oxide-based films for thick insulating layers. This opens plenty of room to introduce new fabrication technologies and new materials for thick insulating layer in Power MEMS.

In this paper, we report the results of an in-depth study on the electrical properties of CYCLOTENE<sup>1</sup>, a spin-on, low dielectric constant polymer derived from benzocyclobutene (BCB). The paper focuses on the electrical properties that have significant impact on the operation of an electric micromotor/generator with CYCLOTENE as the insulating dielectric film. This characterization is useful for application of CYCLOTENE as a dielectric insulating layer in MEMS with a focus on electric micromachines such as micromotors and power microgenerators. The result of this study is suitable in the development of a multi-phase, bottom-drive, variable-capacitance micromotor, with an emphasis on the design and fabrication of the electrical components.

<sup>1</sup>Dow Chemical Company, Midland, MI. Online: <http://www.cyclotene.com>.

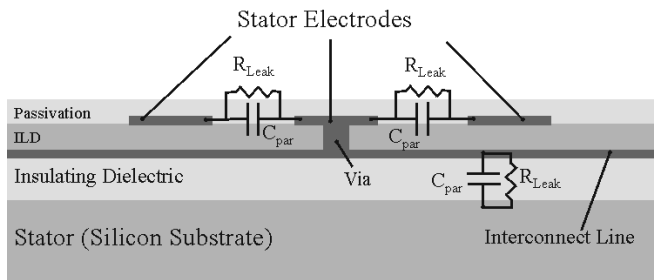


Fig. 1. Cross-section view of the stator in a typical multiphase electric micromachine showing the dielectric insulating layers and the associated parasitic elements. (Dimensions are not to scale).

## II. DIELECTRIC FILMS FOR POWER MEMS

In most electric micromachines, a dielectric film is used to insulate the electrically active components from the substrate. It also serves as the interlevel dielectric (ILD) in multilevel metallization, usually on the electrical stator to insulate metal lines from each other. Fig. 1 illustrates a schematic cross section of a stator in a typical micromachine showing dielectric layers and related parasitic elements. The physical properties of the dielectric film have a major impact on the electrical efficiency and reliability. In this paper, we focus on the electrical properties of the dielectric insulating layer.

A dielectric material must have certain properties to 1) minimize the electrical energy loss; 2) maximize the power conversion capacity; 3) maximize the electrical efficiency; and 4) maximize the device reliability. These features include good electrical properties such as low dielectric constant, high dielectric strength, high volume resistivity, and low dissipation factor, good mechanical properties such as low residual stress, and good process capabilities such as wide range of film thickness, high degree of planarization, low process temperature, and good thermal stability at high temperatures. However, no real dielectric material has all these features. A tradeoff is necessary based on the given application and its target requirements.

Most electric micromachines operate under alternating-current high voltages with some limitations in electrical efficiency and reliability. High-voltage operation is basically limited by electrical breakdown, which is likely to occur in the dielectric insulating layers and the air gap. The electrical efficiency and power conversion capacity are limited by the amount of stored reactive power in the capacitive loads as well as the dielectric loss in the insulating layers. These behaviors are directly related to the electrical properties of the dielectric films used in the device. The parasitic capacitances between the electrical components and the substrate, and also between the adjacent excitation phases contribute to the capacitive loading effects on the electrical power transferred between the electric machine and the power electronic circuits. The dielectric loss in the insulating layers contributes to power dissipation and electrical energy loss. The dielectric loss has two components: the loss associated with leakage currents in the dielectric due to electrons and ions drift currents, and the loss associated with displacement currents due to space charge polarization and dielectric dipole motion. The latter is more important at high frequencies and will not be considered in this paper.

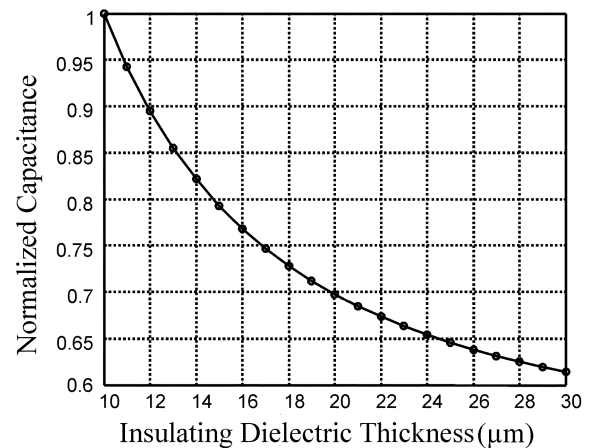


Fig. 2. Simulation of normalized parasitic capacitance per phase between 30 stator electrodes and substrate versus the insulating layer thickness in a six-phase electric micromachine. The capacitance is normalized to its value for a 10- $\mu$ m-thick dielectric layer.

Two key components to maximize the reliability and minimize the electrical energy loss associated with the insulating dielectric layer are the thickness and the dielectric constant ( $k$ ). Fig. 2 shows the result of a finite-element simulation on how the parasitic capacitance between the stator electrodes and substrate of a six-phase electric micromachine changes with the thickness of the insulating layer. The effect of dielectric thickness on device efficiency was also investigated in previously reported work on an electric induction machine, showing a 25% increase in system efficiency if the thickness of the stator dielectric layer is doubled [15]. The parasitic capacitances are also directly proportional to the dielectric constant of the insulating layers. Therefore, it is desired to have a thick, low- $k$  dielectric film for the insulating layer. However, realization of thick films in microfabrication encounters challenging mechanical issues, i.e., a substantial amount of residual stress that can lead to large wafer bow and film cracks. Application of low- $k$  materials faces additional challenges like moisture uptake during device lifetime that degrades breakdown strength and leakage current and thermal instability at high temperatures.

## III. SPIN-ON LOW- $k$ BCB-BASED POLYMERS

Low- $k$  polymers based on BCB [16], [17] are among the promising alternatives to PECVD oxide for variety of applications. These polymers are commercially available from the Dow Chemical Company under the registered trademark called CYCLOTENE, which is a family of thermosetting polymer materials prepared from 1, 3-divinyl-1, 1, 3, 3-tetramethyldisiloxane-bisbenzocyclobutene (DVS-bis-BCB) monomer [18], [19]. The chemical structures of BCB and DVS-bis-BCB are shown in Fig. 3.

CYCLOTENE is available in two categories: dry-etch and photosensitive, both in the form of spin-on solutions. The dry-etch CYCLOTENE comes in different viscosities to obtain cured films in the range of 1 to 26  $\mu$ m thick and contains B-staged (i.e., partially cross-linked) DVS-bis-BCB monomer in mesitylene solvent. The photosensitive CYCLOTENE is also supplied in different viscosities to obtain cured films in the range of 2.5 to 14  $\mu$ m thick and contains a photoactive

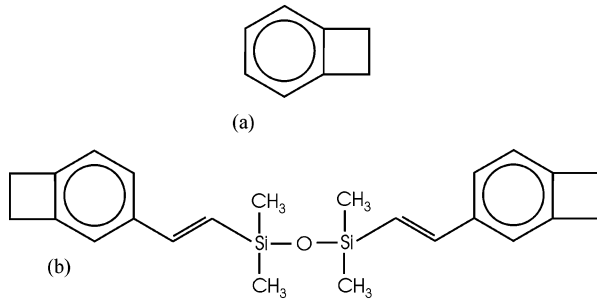


Fig. 3. Chemical structures of (a) BCB and (b) DVS-bis-BCB.

TABLE I  
VISCOSITY AND CURED FILM THICKNESS  
OF DIFFERENT LINES OF CYCLOTENE

CYCLOTENE Solutions	Viscosity (cSt @ 25 °C)	Thickness of Cured Film (μm)
3022-35	14	1.0-2.4
3022-46	52	2.4-5.8
Dry-etch		
3022-57	259	5.7-15.6
3022-63	870	9.5-26.0
XU-71918.30	8.9	1.0-1.5
4022-35	195	2.5-5.0
Photosensitive		
4024-40	350	3.0-7.5
4026-46	1100	7.0-14.0

component in addition to the B-staged monomer and the solvent. The photosensitive CYCLOTENE is negative acting and sensitive to a broad range of UV wavelength including G-line and I-line. Table I shows the available lines of CYCLOTENE and the film thickness ranges. Thinner films can be achieved by diluting the solution with mesitylene, while thicker films can be obtained by spin-casting the solution in multiple layers. Table II summarizes some of the general processing features of CYCLOTENE. Table III shows some of the electrical and mechanical properties of CYCLOTENE based on the previously reported works.

CYCLOTENE was primarily developed as an ILD and passivation coating in microelectronic interconnects and packaging for application in multichip modules (MCM) [20]–[23]. CYCLOTENE features simplified processing, low dielectric constant, high degree of planarization and gap filling, low moisture absorption, and low-temperature cure. Another key feature of CYCLOTENE is that a wide range of film thickness is achievable (up to tens of micrometers). These characteristics were found to be useful in many other microelectronic applications, such as damascene copper interconnects [24], flip-chip solder bumping [25], [26], flat panel displays and charged-coupled devices, optical waveguides [27]–[29], RF high- $Q$  inductors [30], [31], stress buffer and passivation layers [32], and microsensors [33]. The application of CYCLOTENE in MEMS has been mainly limited to packaging and adhesive bonding [34]–[37]. One of the main challenges in application of CYCLOTENE film in MEMS is its integration with conventional MEMS fabrication processes, such as bulk micro-machining which has been addressed in our recent work [38].

Some of the outstanding features of CYCLOTENE, such as low dielectric constant and large film thickness, are well suited for electric micromachinery applications. Numerical

TABLE II  
PROCESSING FEATURES OF DRY-ETCH CYCLOTENE

Process	Method	Details
Surface Treatment	Adhesion Promoter	AP3000
Deposition	Spin-coat	1000-5000 rpm
Soft Cure	Furnace	N <sub>2</sub> , 1h @ 210 °C
Hard Cure	Furnace	N <sub>2</sub> , 1h @ 250 °C
Etching	Plasma	O <sub>2</sub> /CF <sub>4</sub> or O <sub>2</sub> /SF <sub>6</sub>

TABLE III  
PHYSICAL PROPERTIES OF CYCLOTENE

Property	Value	
Electrical	Dielectric Constant	2.65
	Dissipation Factor	0.0008 @ 1 MHz – 10 GHz
	Dielectric Strength	3 × 10 <sup>6</sup> V/cm
	Volume Resistivity	1 × 10 <sup>19</sup> Ω.cm @ 25 °C
Mechanical	Tensile Strength	85 ± 9 MPa (dry-etch) 87 ± 9 MPa (photosensitive)
	Tensile Modulus	2.0 ± 0.2 GPa (dry-etch) 2.9 ± 0.2 GPa (photosensitive)
	Tensile Elongation	8 ± 2.5 % @ break
	Poisson Ratio	0.34
	Residual Stress on Si	28 ± 2 MPa @ 25 °C
	Thermal	Thermal Conductivity
CTE		52 ppm/°C @25-300 °C
T <sub>g</sub>		> 350 °C
Thermal Stability		1.6 % @ 350 °C (weight loss per hour)
Optical	Index of Refraction	1.54 @ 1300-1550 nm (for hard cured films)
	Density of Cured Film	1.05 g/cm <sup>3</sup>
Other	Moisture Uptake	0.13 % @ 81 %RH (dry-etch) 0.14 % @ 84 % RH (photosensitive)
	Shrinkage after Cure	< 5 %
	Planarization	> 90 %

simulations show that if a 15-μm-thick PECVD oxide film is replaced with a 26-μm CYCLOTENE film in the stator of a six-phase electric micromachine, the parasitic capacitive loading of the insulating dielectric film decreases over 40%, which is a remarkable improvement for the electrical efficiency of the machine, not to mention the fabrication difficulties involved in developing a 15-μm-thick PECVD oxide film.

There are two major concerns in using CYCLOTENE films for Power MEMS applications. One concern is the thermal stability of the polymer at operating temperatures of Power MEMS. As Table III shows, the glass transition temperature ( $T_g$ ) of CYCLOTENE is close to 350°C, which is below the requirement of some Power MEMS, especially when the device includes a combustor located close to the electric machine. However, in addition to available methods for cooling down the electrical components to lower temperatures in a high temperature Power MEMS, there are many applications that the operating temperature of the device is well below 350°C. The other concern is whether the small moisture uptake in the CYCLOTENE film degrades the electrical and mechanical properties that might affect the design and the performance of the electric micromachine. Therefore, it is important to characterize the main properties of the dielectric film for the target application. Furthermore, it is essential to investigate the effect of moisture on these properties.

#### IV. ELECTRICAL CHARACTERIZATION OF BCB-BASED POLYMERS

The electrical properties of interest in this paper are the dielectric constant and the current-voltage characteristics of the film. The leakage current and the breakdown voltage can be determined from the  $I$ - $V$  curve. We have also studied the effect of moisture uptake on these properties. Another electrical property of a dielectric material is the dissipation factor (dielectric loss tangent), which becomes important at high frequencies and will not be discussed in this paper.

Since the introduction of BCB-based polymers for microelectronic applications in 1990, there have been a few studies on the electrical characterization of these materials. The method of measurement and the test structures are not completely clear in most of previous studies, and therefore, it is not possible to compare the results. There are also some discrepancies in the reported data for some of the electrical properties. Most studies, with a couple of exceptions, have been done on thin ( $1\ \mu\text{m}$ ) films.

The reported dielectric constant in the literature ranges as high as 3.1 [19]. The nominal dielectric constant of CYCLOTENE is 2.65 as mentioned in [18] and the data specification sheets from the manufacturer. It was also reported to be flat over a wide range of frequencies (1 kHz to 60 GHz) and temperatures ( $25^\circ\text{C}$  to  $200^\circ\text{C}$ ) [18], [20], [22], although it was reported that the dielectric constant changes drastically with cure temperature [39]. Capacitance measurements on free-standing films yielded a dielectric constant of 2.6 to 2.8 [20], [22]. Extraction of the dielectric constant from accumulation capacitance of 1 MHz  $C$ - $V$  curves of metal-insulator-semiconductor capacitors yielded values from 2.2 to 2.8 for cure temperatures from  $200^\circ\text{C}$  to  $350^\circ\text{C}$  [39].

Less data was reported for  $I$ - $V$  characteristics of CYCLOTENE. The nominal value of dielectric strength as mentioned in the specification data sheet from Dow Chemical is  $3 \times 10^6$  V/cm. The dielectric strength measured on  $1.7\ \mu\text{m}$  thin film deposited on silicon substrate was reported to be  $4 \times 10^6$  V/cm while it was measured to be  $2.5 \times 10^6$  V/cm for  $22\ \mu\text{m}$  free standing film [20], [22].

The phenomena of moisture uptake in BCB films was studied in detail using gravimetric measurements [40], however, no electrical characterization was performed in that study. It was also stated that the change in the dielectric constant of BCB-based dielectric polymers under humid conditions is negligible since DVS-bis-BCB has a nonpolar molecular structure [18], although no experimental data was presented.

In this paper, we introduce a method suitable for measuring the dielectric constant and the  $I$ - $V$  characteristics of thick, spin-on dielectric materials. We have used this method to measure the electrical properties of CYCLOTENE and the effect of moisture uptake on these properties.

##### A. Test Devices

The electrical test devices used for this study are interdigitated capacitors (IDCs) with fine finger width and spacing, relatively large finger length, and a large number of fingers. The IDCs are thin metal structures sandwiched between two layers

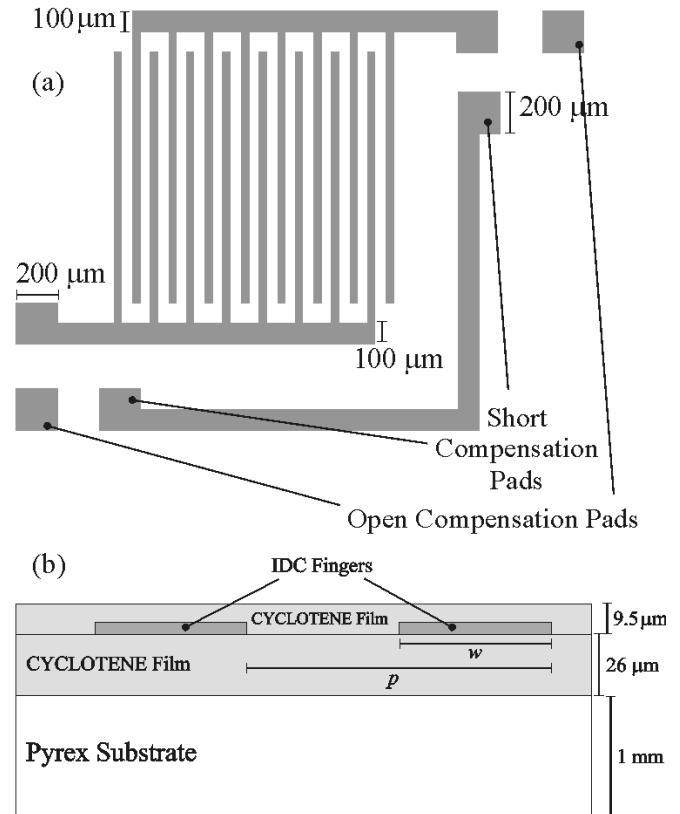


Fig. 4. Schematic views of the designed IDCs: (a) top view and (b) cross-section view. Dimensions are not to scale. The open and short compensation pads are used for elimination of parallel and series parasitic impedances during capacitance measurement.

of dielectric film. There are two reasons that we chose this type of device for our characterization. First, the periodic structure and the size of the designed IDCs are similar to those of the stator electrodes in our electrostatic micromotor; and second, it is easier and faster for the underlying dielectric layer to absorb moisture through the spacing between the fingers in the IDC. This makes the IDC a suitable device to study the effect of the moisture uptake.

Fig. 4 shows the schematics of the top and cross-section views of an IDC. All fabricated IDCs have 500 fingers (250 fingers for each electrode) with equal finger width and spacing (a finger width to pitch ratio of 0.5), four different finger widths,  $1\ \mu\text{m}$ ,  $2\ \mu\text{m}$ ,  $3\ \mu\text{m}$ , and  $4\ \mu\text{m}$ , and two different finger lengths, 1 mm and 10 mm. We have used a 1-mm-thick, 4" Pyrex 7740 wafer as the substrate. Since Pyrex is a nonconducting material, using a Pyrex wafer instead of a silicon wafer minimizes the parasitic elements during the tests. We have experienced difficulties in fabrication when using a 0.5-mm-thick Pyrex wafer due to the wafer bow caused by the residual stress of thick dielectric films; hence, a thicker wafer is preferred.

There are some design considerations when choosing the thickness of the dielectric layers and the thickness of the metal film. The thickness of the bottom and top dielectric films needs to be larger than the pitch of the IDC under test, for reasons that will be discussed in Section V. CYCLOTENE 3022-63 is used as the dielectric under test since it has the highest viscosity providing a maximum of  $26\ \mu\text{m}$  and a minimum of  $9.5\ \mu\text{m}$

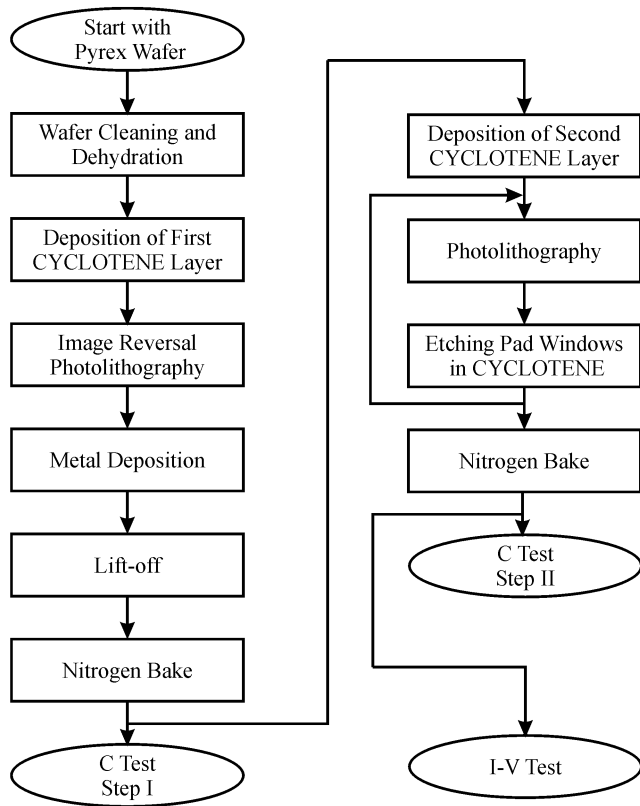


Fig. 5. Process flow for fabrication of test structures showing at what steps the capacitance and current-voltage tests are performed.

film thickness after cure. The bottom and top dielectric films are designed to be  $26\ \mu\text{m}$  and  $9.5\ \mu\text{m}$  thick, respectively, both with a thickness greater than the largest pitch ( $8\ \mu\text{m}$ ). A thicker dielectric top layer led to a more complicated fabrication process. Furthermore, the thickness of the metal film compared to the finger width is an important parameter that affects the capacitance measurements. A metal film of zero thickness is ideal, but if the metal film is too thin, the resistance of IDC electrodes becomes large, leading to difficulties and errors in measurements. Our measurements show that a metal thickness near  $3000\ \text{\AA}$  provides reasonably low resistance electrodes. On the other hand, if the metal thickness is comparable to the finger width, a numerical compensation is necessary when measuring the dielectric constant.

### B. Fabrication

The fabrication process flow of test devices is shown in Fig. 5. As the figure shows, capacitance test step I is performed on an intermediate device before the second layer of CYCLOTENE is deposited. The capacitance test step II and the  $I$ - $V$  test are performed on the final device with two layers of CYCLOTENE. Also note that the sample is baked in a 5 liter/min flow of nitrogen at  $200^\circ\text{C}$  for 2 hours before each test step. The nitrogen bake drives the absorbed moisture out of the CYCLOTENE film.

The test structures are fabricated on a 1-mm-thick, 4" Pyrex 7740 wafer. It is very important that the wafer is cleaned aggressively and dehydrated long enough to remove any organic residues and moisture before deposition of CYCLOTENE. An

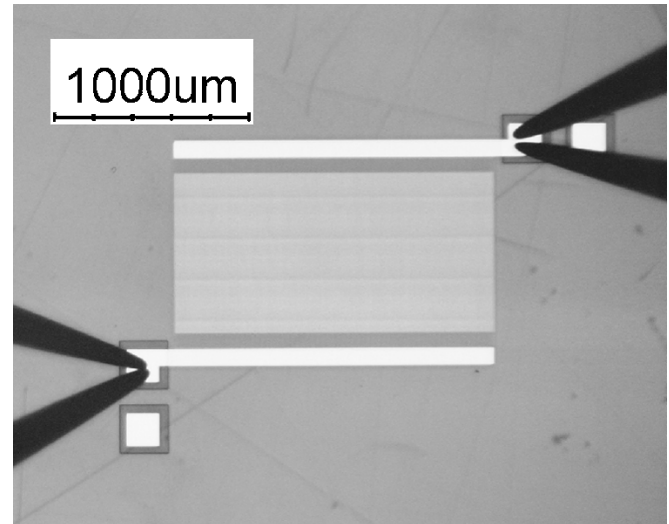


Fig. 6. Optical micrograph of a fabricated IDC with  $2\text{-}\mu\text{m}$  finger width and spacing, and a 1-mm finger length.

adhesion promoter, AP3000 from Dow Chemical, is applied onto the wafer to improve the adhesion of CYCLOTENE to the substrate and a  $26\text{-}\mu\text{m}$ -thick CYCLOTENE 3022-63 film is spun on and cured at  $250^\circ\text{C}$  for 1 hour in the nitrogen flow.

We use a lift-off process to fabricate the IDCs, providing smoother and more accurate metal lines. Furthermore, the advantage of lift-off over a metal etching process in this case is to avoid the exposure of the deposited CYCLOTENE film to metal etchants that contain strong acids. In order to facilitate the lift-off process, an image reversal photolithography is used to pattern AZ5214E photoresist. AZ5214E is a positive-tone photoresist from Clariant Corporation (Muttens, Switzerland). A post-exposure bake at  $125^\circ\text{C}$  for 3 min reverses the tone of this photoresist and a flood exposure with a high dose of  $1200\ \text{mJ}/\text{cm}^2$  makes the unexposed areas soluble in developer. This makes the AZ5214E image reversal process suitable for lift-off, because it reverses not only the pattern but also the profile of the photoresist, providing a re-entrant profile. After photolithography, a 30-s oxygen plasma descumming is performed on the wafer to remove any remaining photoresist residue after development. A Minilock (Trion Technology, Tempe, AZ) plasma etcher is used for descumming at an RF power of 50 W, a chamber pressure of 200 mT, and an oxygen flow of 50 sccm, removing the AZ5214E photoresist at  $3600\ \text{\AA}/\text{min}$ . The metal layers ( $200\ \text{\AA}$  of Cr and  $3000\ \text{\AA}$  of Au) are then deposited using e-beam evaporation and lift-off is performed to fabricate the IDCs.

After the first test step, a second layer of CYCLOTENE 3022-63 with a thickness of  $9.5\ \mu\text{m}$  is spun on and cured in a similar way to the first layer. However, no adhesion promoter is applied prior to the deposition of the second layer. Since the etch selectivity of CYCLOTENE over photoresist etch mask is quite low, we perform two series of photolithography with AZ9245, a positive photoresist from Clariant, and two dry-etching steps to open windows in the CYCLOTENE film for IDC electrode pads. The CYCLOTENE is etched for a total time of 30 min with  $\text{O}_2/\text{CF}_4$  in the plasma etcher at an RF power of 100 W, a chamber pressure of 250 mT, an  $\text{O}_2$

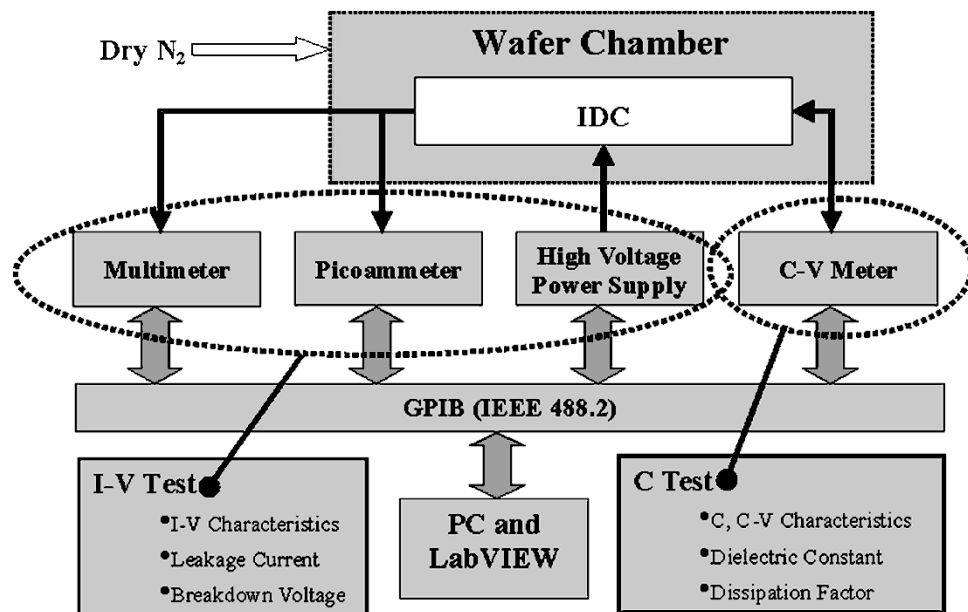


Fig. 7. Block diagram of the electrical test setup for capacitance and  $I$ - $V$  tests. Capacitance and dissipation factor measurements are performed using a 4279A 1-MHz  $C$ - $V$  meter (Agilent, Palo Alto, CA). A high-voltage power supply, a multimeter, and a picoammeter are used to perform  $I$ - $V$  test. The data collection is automated and all instruments are connected to a PC using a GPIB (IEEE 488.2) card and controlled by a LabVIEW (National Instruments, Austin, TX) program.

flow of 90 sccm and a  $CF_4$  flow of 10 sccm. The etch rate of CYCLOTENE is measured to be about  $0.3 \mu\text{m}/\text{min}$  with an etch selectivity of about 0.6 over AZ9245 photoresist.

Separate samples are fabricated for  $C$ - $V$  and  $I$ - $V$  tests. Fig. 6 shows an optical micrograph of a fabricated IDC.

### C. Test Setup

A custom environmental test setup was built to apply humidity stress to the sample under test. The setup is intended to accelerate the moisture uptake in the CYCLOTENE film. The setup is capable of maintaining temperature of  $85^\circ\text{C}$  and relative humidity of 85% RH inside a wafer chamber (see Fig. 8). Dry nitrogen is heated and mixed with steam. The temperature and relative humidity are adjusted by manually controlling the heaters, and flows of nitrogen and steam. Two heaters around the wafer chamber help to prevent condensation inside the chamber. A thermohygrometer reads the temperature and relative humidity.

Fig. 7 shows the block diagram of the electrical test setup consisting of capacitance and  $I$ - $V$  test equipment. The wafer is placed inside a wafer chamber with a constant flow of dry nitrogen at room temperature. The chamber has windows for insertion of probes and thermohygrometer sensor. Fig. 8 shows a close-up view of the chamber.

## V. MEASUREMENT OF DIELECTRIC CONSTANT

In this section, we describe a method that is suitable for measurement of the dielectric constant of any spin-on material provided that it can be spin-coated thicker than the pitch of the IDC under test [41]. The method is based on two capacitance measurements on IDCs and it has advantages over the conventional parallel-plate-capacitor method. This approach is independent of the thickness of the dielectric material under test if it is thick enough. Under some circumstances it can also be independent of the geometrical features of the devices under test. It is very

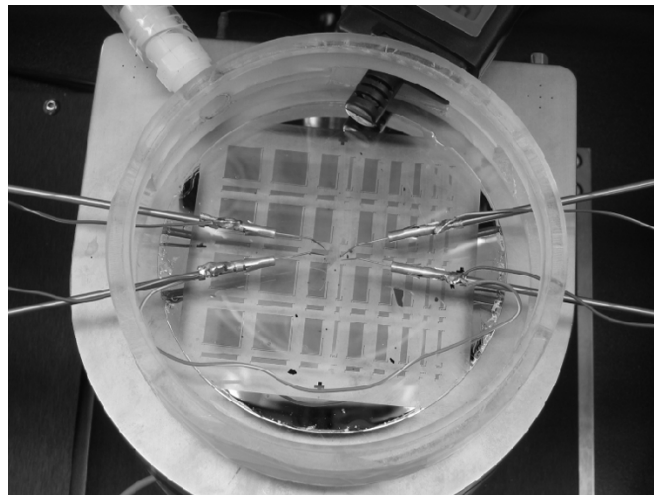


Fig. 8. The wafer chamber for electrical tests under controlled environment enclosing a Pyrex wafer with fabricated IDCs, four test probes, and thermohygrometer sensor. The electrical connections to the devices on the wafer are made using a microwave probe station.

useful to measure the effective dielectric constant over a large area to take into account the fabrication imperfections. This makes the method applicable for large area devices like micro-motors and microgenerators. In addition, the special structure of IDCs makes the study of the effect of moisture uptake easier. We have applied this method to CYCLOTENE films using the fabricated IDCs.

### A. Theory

The capacitance of an ideal IDC can be analytically calculated based on the schematic of Fig. 9 and the following assumptions: 1) number of fingers ( $N$ ) is infinite; 2) finger length ( $L$ ) is infinite; 3) finger thickness ( $t$ ) is zero; 4) dielectric thickness ( $d_1, d_2$ ) is infinite; and 5) the dielectric materials are isotropic.

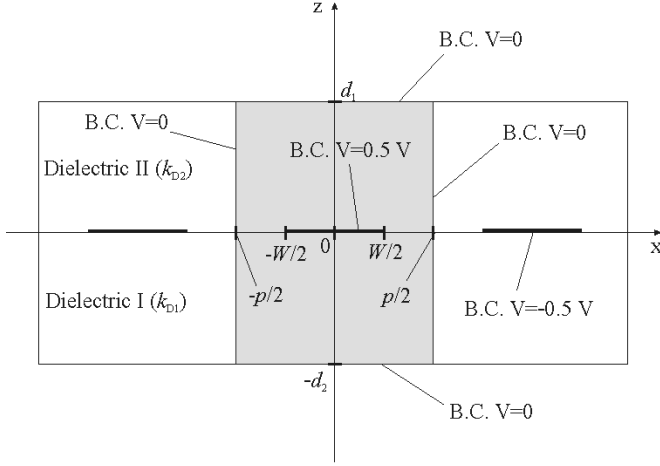


Fig. 9. Schematic cross section of an IDC ( $W$ : finger width,  $p$ : finger pitch) showing the dielectric layers, fingers, and boundary conditions in an ideal IDC. The electric potential between two adjacent fingers is assumed to be 1 V. Due to the symmetric structure, the shaded area is where the Laplace Equation is solved analytically and numerically.

Based on these assumptions, solving the Laplace Equation over the shaded area in Fig. 9 with specified boundary conditions yields the following equation for the capacitance per finger per unit length [42]:

$$C_L = (k_{D1} + k_{D2})\varepsilon_0 \frac{1}{K\left(\cos\frac{\pi W}{2p}\right)} \cdot \sum_{n=0}^{\infty} \frac{1}{2n+1} P_{n-1}\left(\cos\frac{\pi W}{p}\right) \sin\left(\frac{(2n+1)\pi W}{2p}\right) \quad (1)$$

where  $k_{D1}$  and  $k_{D2}$  are the dielectric constants of top and bottom dielectric layers, respectively,  $\varepsilon_0$  is the permittivity of vacuum,  $W$  is the finger width,  $p$  is the finger pitch,  $K$  is the complete elliptic integral of the first kind, and  $P_{n-1}$  is the Legendre Polynomial of the order of  $n$ . A closer look at (1) shows that it can be written in the following form:

$$C_L = (k_{D1} + k_{D2})\varepsilon_0 G_L \left(\frac{W}{p}\right) \quad (2)$$

where  $G_L$  is only a function of IDC finger width to pitch ratio. In other words,  $G_L$  is only a function of geometry, and is independent of the material properties. Under some circumstances (1), and therefore (2), are accurate for nonideal IDCs: 1)  $N$  is large; 2)  $L \gg W$ ; 3)  $t \ll p - W$ ; and 4)  $d_1$  and  $d_2 > p$  [43], [44]. The effect of finite thickness of dielectric layers on the IDC capacitance is analytically shown in the Appendix. With the IDC design of Fig. 4, the analysis predicts an error of 0.03% for an 8- $\mu\text{m}$  pitch and 0.12% for a 10- $\mu\text{m}$  pitch IDC when using (2) to calculate the capacitance of a nonideal IDC with a 26- $\mu\text{m}$  bottom dielectric layer and a 9.5- $\mu\text{m}$  top dielectric layer. This prediction is in agreement with our numerical simulation of the IDC with FEMLAB (COMSOL Inc., Burlington, MA) as seen in Fig. 10. As a result, the capacitance of an IDC can be accurately modeled by (2) if the thickness of dielectric layers is larger than the IDC pitch. This behavior has also been experimentally demonstrated in [41]. Based on the above observations, for an IDC with  $N$  fingers and finger length  $L$ , provided that the above

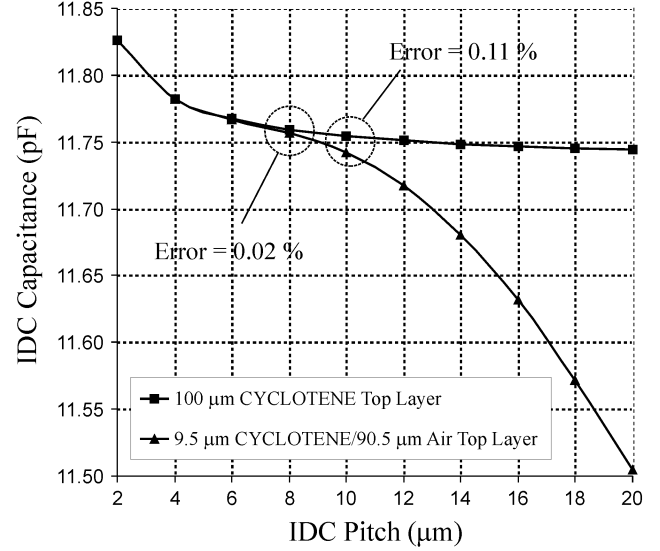


Fig. 10. Two-dimensional finite-element numerical simulation of the capacitance versus pitch in a 500-finger IDC with 1 mm long fingers, showing the effect of CYCLOTENE top layer finite thickness. The simulation is performed based on the IDC design of Fig. 4 and boundary conditions of Fig. 9. The first graph represents the ideal case assuming a very thick (100  $\mu\text{m}$ ) CYCLOTENE layer on top and the second graph is for the IDC design assuming 9.5  $\mu\text{m}$  of CYCLOTENE and 90.5  $\mu\text{m}$  of air on top. As the graphs show, the capacitance of the 8  $\mu\text{m}$  pitch IDC deviates from the ideal case by only 0.02% while as the pitch increases beyond the CYCLOTENE top layer thickness, the deviation blows up drastically. Note that the increase in capacitance at smaller pitches is due to the nonzero finger thickness (0.004  $\mu\text{m}$  in this simulation).

assumptions are met, we can write the total capacitance of the IDC from (2) as

$$C_T = (k_{D1} + k_{D2})\varepsilon_0 N L G_L \left(\frac{W}{p}\right) = (k_{D1} + k_{D2})\varepsilon_0 G_T \left(\frac{W}{p}\right) \quad (3)$$

where we call  $G_T$  the geometry factor of IDCs with  $W/p$  ratio.

The proposed method for measurement of the dielectric constant in this paper is based on (3). Since the geometry factor does not change with material properties, it is possible to extract  $k_{D1}$  or  $k_{D2}$  if the other is known using two capacitance tests (see Fig. 5). In the capacitance test step I, the bottom dielectric layer is CYCLOTENE ( $k_{D2} = k_{BCB}$ ) and the top dielectric layer is dry nitrogen ( $k_{D1} = 1.00058 \cong 1.00$ ), therefore (3) becomes

$$C_I = (k_{BCB} + 1)\varepsilon_0 G_T. \quad (4)$$

In the capacitance test step II, both layers are CYCLOTENE ( $k_{D1} = k_{D2} = k_{BCB}$ ), and therefore we can rewrite (3) as

$$C_{II} = 2k_{BCB}\varepsilon_0 G_T. \quad (5)$$

Then,  $k_{BCB}$  is extracted from (4) and (5):

$$k_{BCB} = \left(\frac{2C_I}{C_{II}} - 1\right)^{-1} \quad (6)$$

where the capacitance ratio must satisfy  $0.5 < C_I/C_{II} < 1$ . For practical low- $k$  materials the ratio range narrows down to  $0.625 < C_I/C_{II} < 0.75$ .

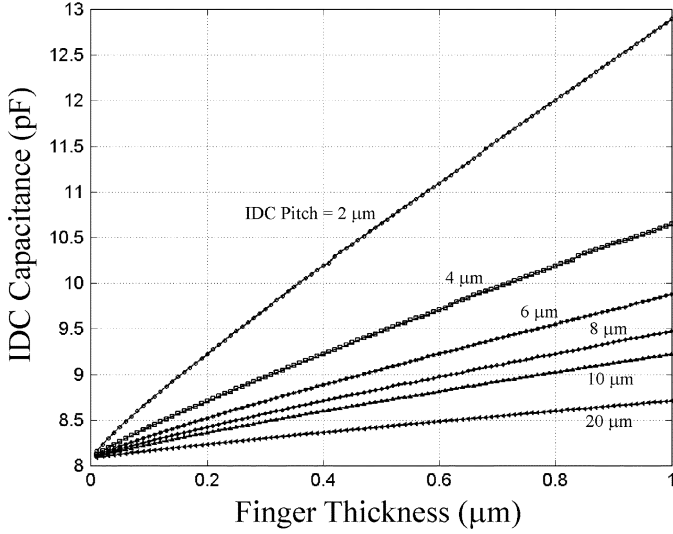


Fig. 11. Estimation for the capacitance of 500-finger IDCs based on the FEA simulation of a single pitch. For IDCs with very thin fingers the capacitance is almost independent of the IDC pitch and finger width as far as the ratio remains constant. As the thickness increases, the capacitance of large-pitch IDCs is less sensitive. The finger length is 1 mm in this simulation.

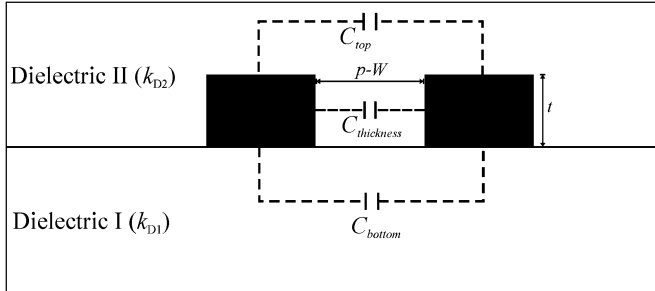


Fig. 12. Schematic cross section of an IDC with thick fingers.

It is possible to compensate for the effect of finger thickness on the capacitance of IDC. Fig. 11 shows the result of simulation with FEMLAB for 500-finger IDCs designed for this study. The capacitance per unit length of IDCs with different finger width is plotted versus the finger thickness. As Fig. 11 shows and (3) verifies, the capacitance of all IDCs is the same when finger thickness is very small. As the finger thickness increases, the capacitance also increases linearly and deviates from ideal IDC case; however, this deviation is more severe for smaller finger widths, as expected. Based on this observation, for an IDC with considerable finger thickness we can add an extra capacitance term associated with a parallel-plate capacitor defined between the walls of fingers (see Fig. 12), therefore (3) is corrected as

$$\begin{aligned} C_T &= C_{top} + C_{bottom} + C_{thickness} \\ &= (k_{D1} + k_{D2})\epsilon_0 G_T \left( \frac{W}{p} \right) + C_{thickness}. \end{aligned} \quad (7)$$

The extra term increases linearly with finger thickness and is proportional to the number of fingers and finger length:

$$C_{thickness} = k_{D2}\epsilon_0 N L \frac{t}{p - W}. \quad (8)$$

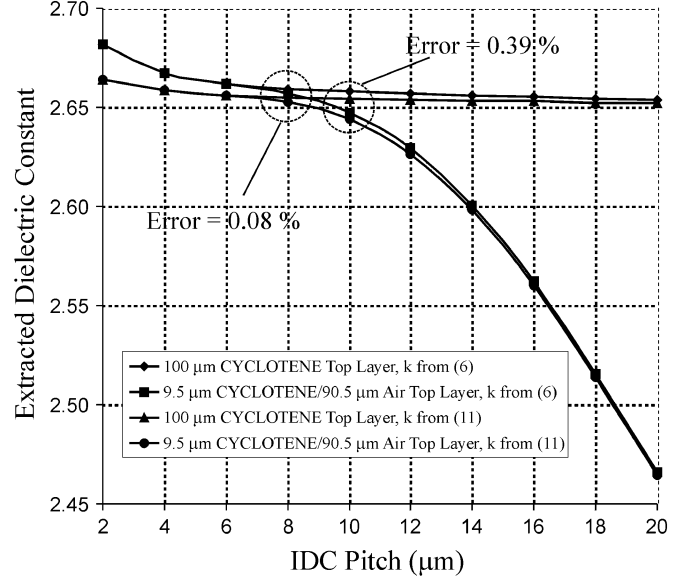


Fig. 13. Two-dimensional finite-element numerical simulation of the extracted dielectric constant versus pitch in a 500-finger IDC with 1 mm long fingers, showing the effect of CYCLOTENE top layer finite thickness. The finger thickness was assumed to be  $0.004 \mu\text{m}$  in this simulation.

Application of this correction to (4) and (5) and considering  $p = 2W$  yields

$$\begin{aligned} C_I &= (k_{BCB} + 1)\epsilon_0 G_T + \epsilon_0 N L \frac{t}{W} \\ &= (k_{BCB} + 1)\epsilon_0 G_T + \epsilon_0 g_T \end{aligned} \quad (9)$$

$$\begin{aligned} C_{II} &= 2k_{BCB}\epsilon_0 G_T + k_{BCB}\epsilon_0 N L \frac{t}{W} \\ &= 2k_{BCB}\epsilon_0 G_T + k_{BCB}\epsilon_0 g_T \end{aligned} \quad (10)$$

where  $g_T = N L t / W$  is the thickness geometry factor depending on the geometrical features of the IDC. Solving (9) and (10) for  $k_{BCB}$  yields

$$k_{BCB} = \frac{C_{II}}{2\epsilon_0 g_T} \left\{ \sqrt{\left( \frac{2C_I}{C_{II}} - 1 - \frac{\epsilon_0 g_T}{C_{II}} \right)^2 + \frac{4\epsilon_0 g_T}{C_{II}}} - \left( \frac{2C_I}{C_{II}} - 1 - \frac{\epsilon_0 g_T}{C_{II}} \right) \right\}. \quad (11)$$

The systematic accuracy of the extracted dielectric constant based on the above method is around 0.1% as long as the IDC pitch is smaller than the dielectric layer thickness. This is shown in Figs. 13 and 14 where the effect of top layer thickness on the dielectric constant is simulated similar to the simulation shown in Fig. 10. Both uncompensated and compensated data are shown. Fig. 13 shows the simulation results for a very thin finger thickness ( $0.004 \mu\text{m}$ ), while in Fig. 14 the finger thickness is assumed the same as in the fabricated IDCs ( $0.32 \mu\text{m}$ ).

## B. Capacitance Test

Capacitance and dissipation factor measurements are performed using an Agilent 4279A 1-MHz  $C-V$  meter. This equipment uses the auto balancing bridge method, a very

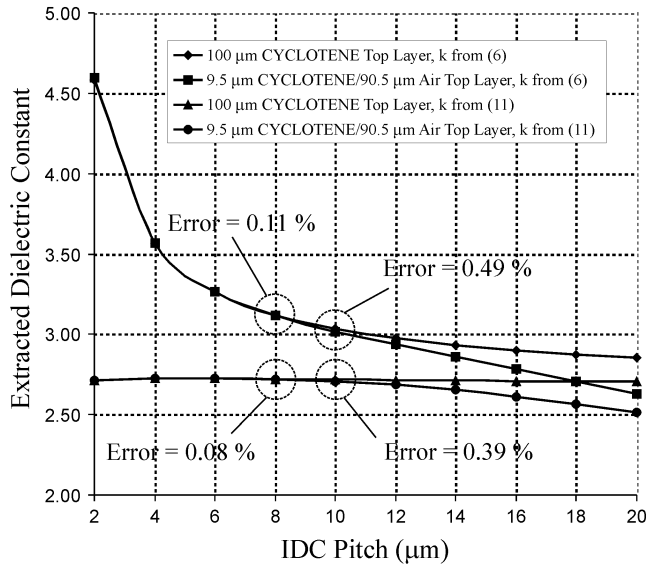


Fig. 14. Two-dimensional finite-element numerical simulation of the extracted dielectric constant versus pitch in a 500-finger IDC with 1 mm long fingers, showing the effect of CYCLOTENE top layer finite thickness. The finger thickness was assumed to be  $0.32 \mu\text{m}$  which is the measured finger thickness in the fabricated IDCs.

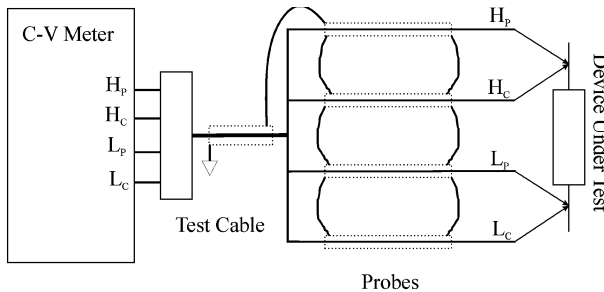


Fig. 15. Four-terminal configuration for capacitance measurement.

accurate method for impedance measurement. A 1 MHz sinusoidal test signal is applied to the high (H) terminals and the current passed through the impedance under test is measured at low (L) terminals. The  $C-V$  meter has four test leads that can be used in two- or four-terminal configuration to measure capacitance and dissipation factor. We have used a four-terminal configuration to minimize the errors associated with mismatches between the test leads, probes, and contact points (see Fig. 15). In addition, a standard 1-m test cable is used to compensate the effect of test cable impedance in the  $C-V$  meter; the amplitude of the test signal is set to 1 V (highest available to minimize the effect of noise). The  $C-V$  meter uses an averaging technique to eliminate random errors. The averaging time and the number of data points for averaging is set to medium mode and 256 (highest number available), respectively. For each set of devices, an open and a short compensation is performed. The open compensation takes into account any stray admittance (in parallel to the device under test) and the short compensation considers any stray impedance (in series with the device under test). Under these circumstances, an accuracy of  $\pm\{0.07\%$  of reading +  $0.03\%$  of full scale $\}$  is expected for measured capacitance. This will lead to an accuracy of about 7 fF ( $\text{fF} = 10^{-15} \text{F}$ ) for 1 mm long IDCs

and about 70 fF for 10 mm long IDCs as long as dissipation factor ( $D$ ) satisfies  $D < 0.1$ . For this reason, all data points with  $D > 0.1$  have been eliminated. Each capacitance data point presented here is the average of 12 measurements with a maximum standard deviation of 2.4 fF. Fig. 16 shows the capacitance values measured at test steps I and II for 1 mm long IDCs. The measurements are performed in a humidity of 0.0 %RH and at room temperature. Fig. 17 shows the extracted dielectric constant of CYCLOTENE before [from (6)] and after [from (11)] thickness correction. The nominal value is plotted for comparison. As Fig. 17 shows, the dielectric constant obtained from (6) is dependent on the pitch of the IDC. This is due to the effect of finger thickness. On the other hand, the dielectric constant obtained from (11) is independent from the geometrical dimensions of the IDC since the effect of thickness is compensated. An average value of 2.49 with a standard deviation of 1.5% is obtained for CYCLOTENE after correction. However, the corrected values still differ from the nominal value of the dielectric constant by 6% on average. A few factors can contribute to this difference. The compensation for the finger thickness is based on a perfectly fabricated IDC according to design specifications; however, there are process imperfections that can change the contribution of the finger thickness to the total capacitance of the IDC. In addition, the imperfections can change the local properties of the dielectric film leading to different values for the dielectric constant.

### C. Effect of Moisture Uptake

The dielectric constant of water is quite high (around 80 at room temperature). This leads to a significant change in the dielectric constant of a polymer if the moisture absorption is appreciable. In order to measure the effect of moisture uptake on CYCLOTENE film, the wafer is exposed to a humidity of 85% RH at  $85^\circ\text{C}$  for 2 hours inside the wafer chamber of the environmental test setup. The capacitance of IDCs is measured using the capacitance test setup before and after the humidity stress. Fig. 18 shows the values of capacitance before and after humidity stress. The change in the capacitance is due to the change in the dielectric constant as a result of moisture uptake in the CYCLOTENE film. The measurements show that the dielectric constant increases by 1.2% on average. As a result, the characteristics of CYCLOTENE as a low- $k$  material exhibit a small change following moisture uptake. In the long term, this is an important and useful feature that helps with the reliability of BCB-based micromachines.

## VI. MEASUREMENT OF $I-V$ CHARACTERISTICS

### A. Theory

Most nonconducting solids exhibit a nonlinear voltage-dependent resistivity at high electric field so that with further increase in the applied voltage the leakage current increases more rapidly. At a certain critical voltage, the current becomes unstable and rises rapidly. At this point the resistance falls to a very low value and the solid acts like a conducting material. This critical voltage is called the breakdown voltage. One important characteristic of this phenomenon is that the properties of the solid do not recover if the applied voltage is removed. This is

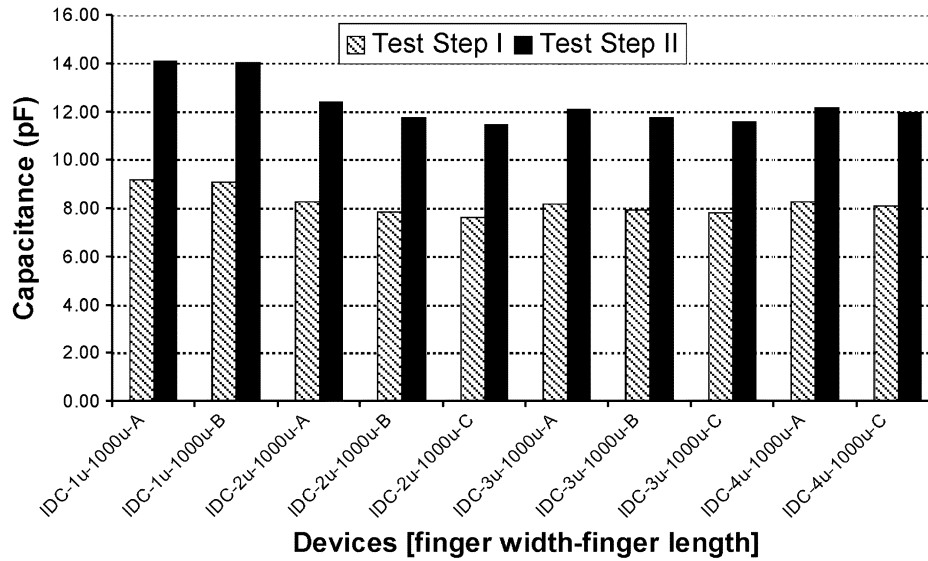


Fig. 16. Capacitance values measured at test steps I and II for 1 mm long IDCs at humidity = 0.0 %RH and room temperature.

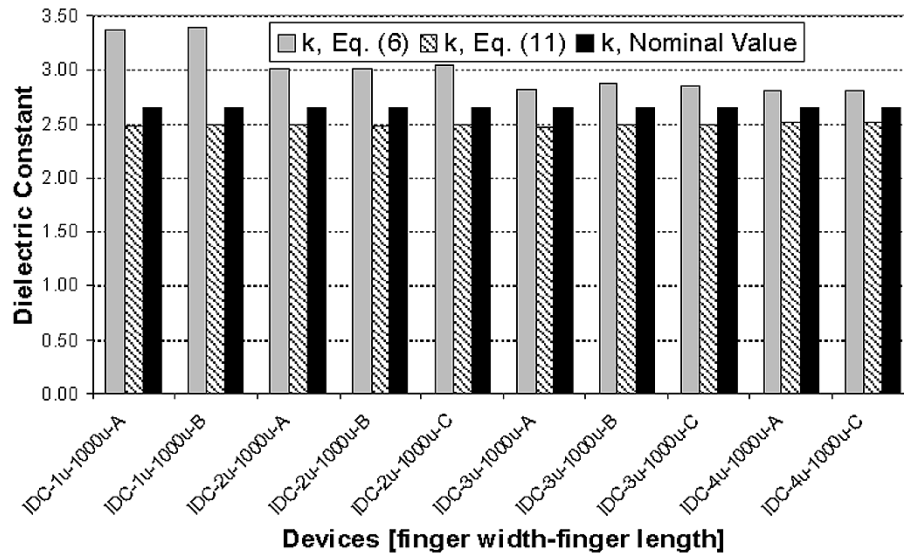


Fig. 17. Dielectric constant of CYCLOTENE without and with finger thickness compensation extracted from (6) and (11), respectively.

a notion of a permanent damage to the solid. In most cases, a structural defect in the solid provides a path with minimal resistance for current. In some cases, the thermal instability of certain sites in the solid triggers a thermal runaway process that eventually leads to breakdown. For some solids, the  $I-V$  curve is fit to one of the following exponential functions [45]:

$$I = Ae^{\alpha V} \quad (12)$$

$$I = Ae^{Be^{\alpha V}} \quad (13)$$

where  $A$ ,  $B$ , and  $\alpha$  are constants. The characteristic difference between (12) and (13) is that (13) features a very sharp increase in the current at the breakdown voltage while the transition in (12) is smoother.

#### B. $I-V$ Test and Effect of Moisture Uptake

Fig. 19 shows the circuit with which the  $I-V$  characteristic of IDCs has been measured. The accuracy of the picoammeter is 0.1 pA. All signals, especially in the input of the picoammeter,

are shielded using coaxial cables to minimize the effect of noise. Since the level of applied voltage is high, the accuracy of voltage measurement is not crucial. The  $I-V$  characteristics are measured with stepping up the applied voltage in 10-V increments, holding the voltage at each step until the change in current is undetectable, and measuring the current. This is repeated until the current rises suddenly. Therefore, the last data point plotted in each graph is one step immediately before breakdown. The  $I-V$  characteristics have also been measured after a humidity stress of 85% RH at 85°C. Fig. 20 shows the measured results for 1 mm long IDCs with 2 and 3  $\mu\text{m}$  finger width, respectively. Exponential curve fits similar to (12) and (13) are also shown on the plots. As it is seen, the  $I-V$  characteristic follows (12) at low voltages and as the voltage increases, it deviates from the exponential curve. On the other hand, (13) predicts the  $I-V$  characteristics very well at low and high voltages.

As Fig. 20 shows, the breakdown strength of dry CYCLOTENE is about 225 V/ $\mu\text{m}$  for 2- $\mu\text{m}$  finger spacing and

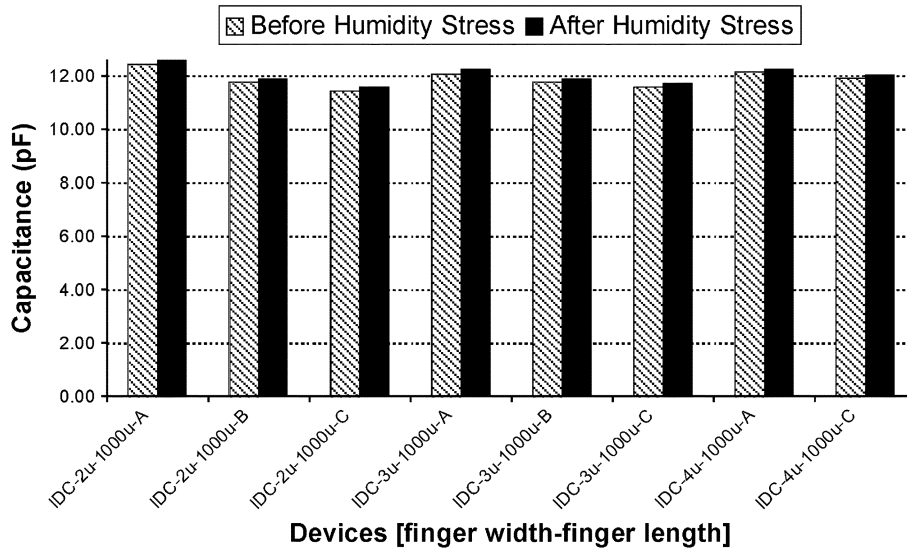


Fig. 18. Capacitance values before and after a humidity stress of 85% RH at 85°C for 2 hours.

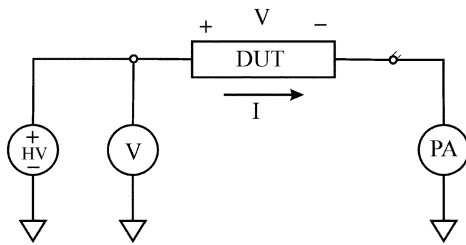


Fig. 19. Circuit for measurement of  $I$ - $V$  characteristics. The voltage is applied to the device under test (DUT) using a high voltage (HV) power supply. The voltage is measured with a digital multimeter, and the current is measured with a picoammeter. The internal current limit of the HV power supply limits the current in case of breakdown.

about  $320 \text{ V}/\mu\text{m}$  for  $3\text{-}\mu\text{m}$  finger spacing. This is comparable to the nominal value of  $300 \text{ V}/\mu\text{m}$  from Table III. On the other hand, for CYCLOTENE after the humidity stress the breakdown strength drops drastically to about  $100 \text{ V}/\mu\text{m}$  for  $2\text{-}\mu\text{m}$  finger spacing and to  $180 \text{ V}/\mu\text{m}$  for  $3\text{-}\mu\text{m}$  finger spacing. The leakage current depends on the applied voltage and finger spacing. The leakage current of dry CYCLOTENE ranges from  $0.1$  to  $6.2 \text{ pA}$  for  $2\text{-}\mu\text{m}$  finger spacing and from  $0.1$  to  $53.4 \text{ pA}$  for  $3\text{-}\mu\text{m}$  finger spacing. After the humidity stress, the increase in the leakage current can be as large as one order of magnitude depending on the applied voltage. As these measurements show, the breakdown strength of CYCLOTENE film depends on the geometry of the device under test and absorption of moisture. We believe that the size and the structure of the device are important factors in the likelihood of electrical failure since these factors contribute to the nature and number of defects and imperfections in the dielectric film. We also believe that moisture helps to form or enhance the conducting paths inside the dielectric material so that even with very small moisture absorption the breakdown strength of the dielectric film remarkably decreases. As seen in Fig. 18, the leakage current is also different by one order of magnitude for different finger spacing. This is because the IDC with larger finger spacing breaks at

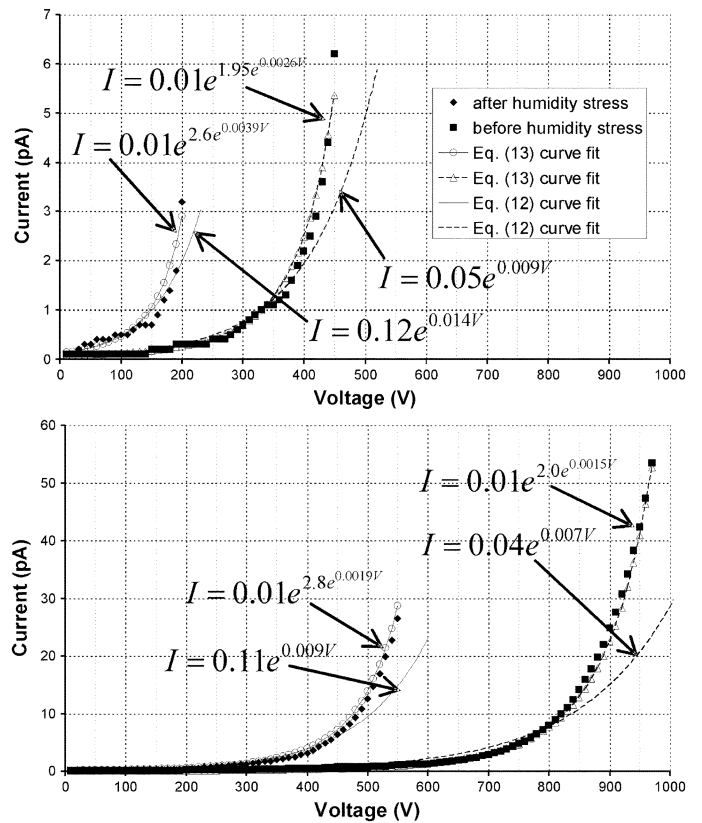


Fig. 20.  $I$ - $V$  characteristics of  $1 \text{ mm}$  long IDCs before and after humidity stress with exponential curve fitting based on (12) and (13),  $2 \mu\text{m}$  finger spacing (top), and  $3 \mu\text{m}$  finger spacing (bottom).

higher voltages where the resistance of the dielectric film has dropped even more, leading to a higher leakage current.

The drastic change in the  $I$ - $V$  characteristics of CYCLOTENE after moisture uptake can lead to reliability issues in BCB-based micromachines, specifically limitation of the maximum operating voltage and occurrence of the early breakdown in humid environment. These results, however, provide

designers with specific knowledge to design and fabricate reliable micromachines using BCB polymers.

## VII. CONCLUSION

In this paper, we have discussed the role of dielectric materials in Power MEMS applications such as electric micromotors and microgenerators. We have also described the effect of dielectric properties of the insulating layer on the electrical performance of micromachines and the importance of electrical characterization of dielectric materials for these applications. It has been stated that a thick dielectric film with a low dielectric constant is desirable since it helps with reduction of electrical energy loss. We have introduced CYCLOTENE, a spin-on, low- $k$ , BCB-based polymer for use in electric micromachines as insulating dielectric layer and interlevel dielectric. We have also introduced a novel approach for measurement of the electrical properties of thick, spin-on dielectrics and studied the effect of moisture uptake. These properties include the dielectric constant and the  $I$ - $V$  characteristics. The tests have been performed on fabricated IDCs that are suitable for this study. The dielectric constant of CYCLOTENE has been extracted from two steps of capacitance measurement and the  $I$ - $V$  characteristics have been measured. The effect of moisture uptake has been studied by applying humidity stress to the film in an environmental test setup built for this study. The experimental results show that the electrical properties of the CYCLOTENE film depend on the structural aspects of the design that can change the process and operational conditions. Moisture uptake also changes the electrical properties. Furthermore, the dielectric constant is proved to be less sensitive to these parameters while the breakdown strength and leakage current can be drastically affected by the design, process, and environmental parameters. Therefore, in the design of electric micromachines using BCB-based polymers, extreme care must be taken in specifying a maximum rating for the operation voltage since the electrical reliability is directly influenced by moisture absorption. The electrical efficiency of the device, on the other hand, is not affected considerably by moisture uptake.

## APPENDIX

In this Appendix, we analytically show the effect of finite thickness of the dielectric layers on the capacitance of an IDC. We assume that the IDC is sandwiched between two finite-thickness dielectric layers with a substrate ( $k = k_S$ ) below and air ( $k = 1$ ) above as depicted in Fig. 4, as well as infinite number of fingers, infinite finger length, and zero finger thickness. By solving the Laplace Equation over the shaded area in Fig. 9 with the specified boundary conditions,  $C_L$  can be written as

$$C_L = \frac{\epsilon_0}{2} \sum_{n=0}^{\infty} \sin\left(\frac{(2n+1)\pi W}{2p}\right) \cdot \left\{ A_n k_{D1} \left[ 1 - \frac{k_{D1}-1}{k_{D1}+1} \exp\left(-\frac{2(2n+1)\pi d_1}{p}\right) \right] + B_n k_{D2} \left[ 1 - \frac{k_{D2}-k_S}{k_{D2}+k_S} \exp\left(-\frac{2(2n+1)\pi d_2}{p}\right) \right] \right\} \quad (14)$$

where  $A_n$  and  $B_n$  are constants satisfying the following equations:

$$A_n \left[ 1 + \frac{k_{D1}-1}{k_{D1}+1} \exp\left(-\frac{2(2n+1)\pi d_1}{p}\right) \right] = B_n \left[ 1 + \frac{k_{D2}-k_S}{k_{D2}+k_S} \exp\left(-\frac{2(2n+1)\pi d_2}{p}\right) \right] \quad (15)$$

$$\sum_{n=0}^{\infty} \frac{(2n+1)\pi}{p} \cos\left(\frac{(2n+1)\pi x}{p}\right) \cdot \left\{ A_n k_{D1} \left[ 1 - \frac{k_{D1}-1}{k_{D1}+1} \exp\left(-\frac{2(2n+1)\pi d_1}{p}\right) \right] + B_n k_{D2} \left[ 1 - \frac{k_{D2}-k_S}{k_{D2}+k_S} \exp\left(-\frac{2(2n+1)\pi d_2}{p}\right) \right] \right\} = 0 \quad (16)$$

if  $W/2 \leq x \leq p/2$ , and

$$\sum_{n=0}^{\infty} A_n \cos\left(\frac{(2n+1)\pi x}{p}\right) \cdot \left[ 1 + \frac{k_{D1}-1}{k_{D1}+1} \exp\left(-\frac{2(2n+1)\pi d_1}{p}\right) \right] = 1 \quad (17)$$

$$\sum_{n=0}^{\infty} B_n \cos\left(\frac{(2n+1)\pi x}{p}\right) \cdot \left[ 1 + \frac{k_{D2}-k_S}{k_{D2}+k_S} \exp\left(-\frac{2(2n+1)\pi d_2}{p}\right) \right] = 1 \quad (18)$$

if  $0 \leq x \leq W/2$ . It can be shown that the asymptotic solution when  $d_1$  and  $d_2$  approach infinity is same as (1). Assuming identical bottom and top dielectrics ( $k_{D1} = k_{D2} = k_D$ ) and large  $d_2$ , we can rewrite (14)–(18) as

$$C_L = k_D \epsilon_0 \sum_{n=0}^{\infty} A_n \sin\left(\frac{(2n+1)\pi W}{2p}\right) \quad (19)$$

$$B_n = A_n \left[ 1 + \frac{k_D-1}{k_D+1} \exp\left(-\frac{2(2n+1)\pi d_1}{p}\right) \right] \quad (20)$$

$$\sum_{n=0}^{\infty} A_n (2n+1) \cos\left(\frac{(2n+1)\pi x}{p}\right) \cdot \frac{k_D-1}{k_D+1} \exp\left(-\frac{2(2n+1)\pi d_1}{p}\right) = 0 \quad (21)$$

$$\sum_{n=0}^{\infty} A_n \cos\left(\frac{(2n+1)\pi x}{p}\right) \cdot \left[ 1 + \frac{k_D-1}{k_D+1} \exp\left(-\frac{2(2n+1)\pi d_1}{p}\right) \right] = 1. \quad (22)$$

The exponential term in (21) and (22) can be used to estimate the relative difference between the asymptotic and nonasymptotic values of  $C_L$  if  $d_1$  is large enough

$$\frac{\Delta C_L}{C_L} \cong \frac{k_D-1}{k_D+1} \exp\left(-\frac{2(2n+1)\pi d_1}{p}\right). \quad (23)$$

Specifically, if  $k_D = 2.65$  and  $d_1 > p$ , (23) yields  $(\Delta C_L/C_L) < 0.001$ .

## ACKNOWLEDGMENT

The authors would like to thank T. C. Loughran and N. A. Ballew from the clean room facilities at the University of Maryland for their help with the fabrication of the test devices.

## REFERENCES

- [1] A. H. Epstein, S. D. Senturia, G. Anathasuresh, A. A. Ayón, K. Breuer, K.-S. Chen, F. E. Ehrich, G. Gauba, R. Ghodssi, C. Groshenry, S. A. Jacobson, J. H. Lang, C.-C. Lin, A. Mehra, J. O. Mur-Miranda, S. F. Nagle, D. J. Orr, E. Piekos, M. A. Schmidt, G. Shirley, S. M. Spearing, C. S. Tan, Y.-S. Tzeng, and I. A. Waitz, "Power MEMS and microengines," in *Dig. Tech. Papers 9th Int. Conf. Solid-State Sensors and Actuators (Transducers'97)*, vol. 2, Chicago, IL, 1997, pp. 753–756.
- [2] A. H. Epstein, S. A. Jacobson, J. M. Protz, and L. G. Fréchette, "Shirt-button-sized gas turbines: The engineering challenges of micro high speed rotating machinery," in *Proc. 8th Int. Symp. Transport Phenomena and Dynamics of Rotating Machinery (ISROMAC'8)*, Honolulu, HI, 2000.
- [3] A. P. London, A. A. Ayón, A. H. Epstein, S. M. Spearing, T. Harrison, Y. Peles, and J. L. Kerrebrock, "Microfabrication of a high pressure bipropellant rocket engine," *Sensors Actuators A*, vol. 92, pp. 351–357, 2001.
- [4] P. Dario, M. C. Carozza, C. Stefanini, and S. D'Attanasio, "A mobile microrobot actuated by a new electromagnetic wobble micromotor," *IEEE/ASME Trans. Mechatron.*, vol. 3, pp. 9–16, 1998.
- [5] L.-S. Fan, Y.-C. Tai, and R. S. Muller, "Integrated movable micromechanical structures for sensors and actuators," *IEEE Trans. Electron Devices*, vol. ED-35, pp. 724–730, 1988.
- [6] —, "IC-processed electrostatic micro-motors," in *IEDM Tech. Dig.*, San Francisco, CA, 1988, pp. 666–669.
- [7] T. A. Lober and R. T. Howe, "Surface-micromachining processes for electrostatic microactuator fabrication," in *IEEE Solid-State Sensor and Actuator Workshop Tech. Dig.*, Hilton Head Island, SC, 1988, pp. 59–62.
- [8] M. Mehregany, K. J. Gabriel, and W. S. N. Trimmer, "Integrated fabrication of polysilicon mechanisms," *IEEE Trans. Electron Devices*, vol. ED-35, pp. 719–723, 1988.
- [9] Y.-C. Tai, L.-S. Fan, and R. S. Muller, "IC-processed micro-motors: Design, technology, and testing," in *Proc. IEEE Micro Electro Mechanical Systems: An Investigation of Micro Structures, Sensors, Actuators, Machines and Robots*, Salt Lake City, UT, 1989, pp. 1–6.
- [10] R. Ghodssi, L. G. Frechette, S. F. Nagle, X. Zhang, A. A. Ayón, S. D. Senturia, and M. A. Schmidt, "Thick buried oxide in silicon (TBOS): An integrated fabrication technology for multi-stack wafer-bonded MEMS processes," in *Dig. Tech. Papers 10th Int. Conf. Solid-State Sensors and Actuators (Transducers'99)*, Sendai, Japan, 1999, pp. 1456–1459.
- [11] X. Zhang, R. Ghodssi, K.-S. Chen, A. A. Ayón, and S. M. Spearing, "Residual stress characterization of thick PECVD TEOS film for power MEMS applications," *Tech. Dig. Solid-State Sensor and Actuator Workshop*, pp. 316–319, 2000.
- [12] X. Zhang, K.-S. Chen, R. Ghodssi, A. A. Ayón, and S. M. Spearing, "Residual stress and fracture in thick tetraethylorthoiclate (TEOS) and silane-based PECVD oxide films," *Sensors Actuators A*, vol. 91, pp. 373–380, 2001.
- [13] K.-S. Chen, J.-Y. Chen, and S.-Y. Lin, "Fracture analysis of thick plasma-enhanced chemical vapor deposited oxide films for improving the structural integrity of power MEMS," *J. Micromech. Microeng.*, vol. 12, pp. 714–722, 2002.
- [14] X. Zhang, K.-S. Chen, and S. M. Spearing, "Thermo-mechanical behavior of thick PECVD oxide films for power MEMS applications," *Sensors Actuators A*, vol. 103, pp. 263–270, 2003.
- [15] S. F. Nagle and J. H. Lang, "A micro-scale electric-induction machine for a micro gas turbine generator," in *Proc. 27th Annu. Meeting Electrostatic Society of America*, Boston, MA, 1999.
- [16] R. A. Kirchhoff and K. J. Bruza, "Benzocyclobutenes in polymer synthesis," *Progr. Polymer Sci.*, vol. 18, pp. 85–185, 1993.
- [17] M. F. Farona, "Benzocyclobutenes in polymer chemistry," *Progr. Polymer Sci.*, vol. 21, pp. 505–555, 1996.
- [18] M. E. Mills, P. Townsend, D. Castillo, S. Martin, and A. Achen, "Benzocyclobutene (DVS-BCB) polymer as an interlayer dielectric (ILD) material," *Microelectron. Eng.*, vol. 33, pp. 327–334, 1997.
- [19] H. Hendricks, "Low dielectric constant materials for IC intermetal dielectric applications: A status report on the leading candidates," in *Materials Research Society Symp. Proc.: Low-Dielectric Constant Materials II*, Boston, MA, 1997, pp. 3–14.
- [20] D. C. Burdeaux, P. H. Townsend, J. N. Carr, and P. Garrou, "Benzocyclobutene (BCB) dielectrics for the fabrication of high density, thin film multichip modules," *J. Electron. Mater.*, vol. 19, pp. 1357–1366, 1990.
- [21] M. J. Berry, T. G. Tessier, I. Turlik, G. M. Adema, D. C. Burdeaux, J. N. Carr, and P. Garrou, "Benzocyclobutene as a dielectric for multichip module fabrication," in *Proc. 40th Electronic Components and Technology Conf.*, vol. 1, Las Vegas, NV, 1990, pp. 746–750.
- [22] R. W. Johnson, T. L. Phillips, W. K. Weidner, S. F. Hahn, D. C. Burdeaux, and P. H. Townsend, "Benzocyclobutene interlayer dielectrics for thin film multichip modules," *IEEE Trans. Compon., Hybrids, Manufact. Technol.*, vol. 13, pp. 347–352, 1990.
- [23] A. J. G. Strandjord, R. H. Heistand, P. Garrou, and T. G. Tessier, "A photosensitive-BCB on laminate technology (MCM-LD)," in *Proc. 44th Electronic Components and Technology Conf.*, Washington, DC, 1994, pp. 374–386.
- [24] D. T. Price, R. J. Gutmann, and S. P. Murarka, "Damascene copper interconnects with polymer ILDs," *Thin Solid Films*, vol. 308–309, pp. 523–528, 1997.
- [25] Y. Ida, P. E. Garrou, A. J. G. Strandjord, S. L. Cummings, W. B. Rogers, M. J. Berry, and S. R. Kisting, "Processing, transfer solder bumping, chip attachment, and testing of a thin film Cu/photo-BCB MCM-D," in *Proc. 18th IEEE/CPMT Int. Electronic Manufacturing Technology Symp.*, Omiya, Japan, 1995, pp. 441–444.
- [26] L. A. Keser, R. Bajaj, and T. Fang, "Redistribution and bumping of a high I/O device for flip chip assembly," *IEEE Trans. Adv. Packag.*, vol. 23, pp. 3–8, 2000.
- [27] C. F. Kane and R. R. Krchnavek, "Benzocyclobutene optical waveguides," *IEEE Photon. Technol. Lett.*, vol. 7, pp. 535–537, 1995.
- [28] S. Wolff, A. R. Giehl, M. Renno, and H. Fouckhardt, "Metallic waveguide mirrors in polymer film waveguides," *Appl. Phys. B*, vol. 73, pp. 623–627, 2001.
- [29] S. Wolff, A. Grosse, H.-J. Schimper, A. R. Giehl, M. Kuhnke, and R. Grote, "Technology and realization of metallic curved waveguide mirrors in polymer film waveguides based on anisotropic plasma etching," *J. Vacuum Sci. Technol. A*, vol. 19, pp. 87–89, 2001.
- [30] A. Okubora, T. Ogawa, T. Hirabayashi, T. Kosemura, T. Ogino, H. Nakayama, Y. Oya, Y. Nishitani, and Y. Asami, "A novel integrated passive substrate fabricated directly on an organic laminate for RF applications," in *Proc. 52nd Electronic Components and Technology Conf.*, San Diego, CA, 2002, pp. 672–675.
- [31] X. Huo, K. J. Chen, and P. C. H. Chan, "Silicon-based high-Q inductors incorporating electroplated copper and low-k BCB dielectric," *IEEE Electron Device Lett.*, vol. 23, pp. 520–522, 2002.
- [32] A. J. G. Strandjord, W. B. Rogers, Y. Ida, R. R. De Vellis, S. Shiao, E. S. Moyer, D. M. Scheck, and P. E. Garrou, "Photosensitive benzocyclobutene for stress-buffer and passivation applications (one mask manufacturing process)," in *Proc. 47th Electronic Components and Technology Conf.*, San Jose, CA, 1997, pp. 1260–1268.
- [33] C. Laville and C. Pellet, "Interdigitated humidity sensors for a portable clinical microsystem," *IEEE Trans. Biomed. Eng.*, vol. 42, pp. 1162–1167, 2002.
- [34] F. Niklaus, P. Enoksson, E. Kalvesten, and G. Stemme, "Void-free full wafer adhesive bonding," in *Proc. IEEE 13th Int. Conf. Micro Electro Mechanical Systems*, Miyazaki, Japan, 2000, pp. 247–252.
- [35] —, "Low-temperature full wafer adhesive bonding," *J. Micromech. Microeng.*, vol. 11, pp. 100–117, 2001.
- [36] T.-K. A. Chou and K. Najafi, "3D MEMS fabrication using low-temperature wafer bonding with benzocyclobutene (BCB)," in *Proc. 11th Int. Conf. Solid-State Sensors and Actuators (Transducers'01, Eurosensors XV)*, vol. 2, Munich, Germany, 2001, pp. 1570–1573.
- [37] T.-K. A. Chou, K. Najafi, M. O. Muller, L. P. Bernal, and P. D. Washabaugh, "High-density micromachined acoustic ejector array for micro propulsion," in *Proc. 11th Int. Conf. Solid-State Sensors and Actuators (Transducers'01, Eurosensors XV)*, vol. 2, Munich, Germany, 2001, pp. 1570–1573.
- [38] N. Ghalichechian, A. Modafe, and R. Ghodssi, "Integration of silicon anisotropic wet etching and BCB processes," presented at the AVS 50th Int. Symp., Baltimore, MD, 2003.
- [39] S. Sivoththaman, R. Jeyakumar, L. Ren, and A. Nathan, "Characterization of low permittivity (low-k) polymeric dielectric films for low temperature device integration," *J. Vacuum Sc. Technol. A*, vol. 20, pp. 1149–1153, 2002.
- [40] H. Pranjoto and D. D. Denton, "Moisture uptake of bisbenzocyclobutene (BCB) films for electronic packaging applications," in *Materials Research Society Symp. Proc.: Electronic Packaging Materials Science V*, Boston, MA, 1990, pp. 295–302.

- [41] A. Modafe, N. Ghalichechian, B. Kleber, and R. Ghodssi, "A new approach to electrical characterization of spin-on dielectrics for power MEMS applications," presented at the AVS 49th Int. Symp., Denver, CO, 2002.
- [42] S. G. Joshi and R. M. White, "Excitation and detection of surface elastic waves in piezoelectric crystals," *J. Acoust. Soc. Amer.*, vol. 46, pp. 17–27, 1969.
- [43] S. R. Ponamgi and H.-S. Tuan, "Theoretical calculation of capacitance of an IDT over a piezoelectric layered structure," *IEEE Trans. Sonics Ultrasonics*, vol. SU-21, pp. 125–127, 1974.
- [44] G. W. Farnell, I. A. Cermak, C. P. Silvester, and S. K. Wong, "Capacitance and field distribution for interdigital surface-wave transducers," *IEEE Trans. Sonics Ultrasonics*, vol. SU-17, pp. 188–195, 1970.
- [45] S. Whitehead, *Dielectric Phenomena, III.—Breakdown of Solid Dielectrics*. New York: Van Nostrand, 1932, p. 21.

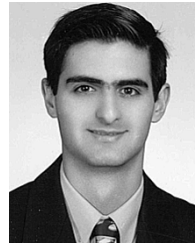


**Alireza Modafe** (S'01) was born in Lahijan, Iran, in 1970. He received the B.S. degree in electrical engineering from Sharif University of Technology, Tehran, Iran, in 1993 and the M.S. degree in electrical engineering from Iran University of Science and Technology, Tehran, in 1997. His M.S. thesis was focused on development of a test system for deep-level transient spectroscopy (DLTS) of charge carrier traps in semiconductors. He is currently pursuing the Ph.D. degree in the Department of Electrical and Computer Engineering, University of

Maryland (UMD), College Park.

He joined the MEMS Sensors and Actuators Laboratory (MSAL) in the Department of Electrical and Computer Engineering, UMD, in August 2000. His research is focused on development of power microelectromechanical devices such as electric micromotors and microgenerators using microball bearing technology and spin-on low- $k$  dielectric polymers.

Mr. Modafe received the 2002 Spring MEMS Alliance Workshop Best Poster Award and the 2002 AVS Graduate Research Award. Mr. Modafe is a member of the American Vacuum Society (AVS) and the Materials Research Society (MRS), and an associate member of Sigma Xi, The Scientific Research Society.



**Nima Ghalichechian** (S'99) was born in Tehran, Iran, in 1978. He received the B.S. degree in electrical engineering from Amirkabir Institute of Technology (Tehran Polytechnique), Tehran, in 2001. His B.S. thesis was focused on design of a maximum power point tracking regulator for photovoltaics. He started his graduate studies in January 2002 at the University of Maryland (UMD), College Park, where he is currently pursuing the Ph.D. degree in electrical engineering.

He joined the MEMS Sensors and Actuators Laboratory (MSAL) in the Department of Electrical and Computer Engineering, UMD, in September 2002. His research area is currently focused on MEMS-based electrostatic micromachines.

Mr. Ghalichechian is a member of the American Association for the Advancement in Science (AAAS) and an associate member of Sigma Xi, The Scientific Research Society.

**Benjamin Kleber** received the B.S. degrees in physics and electrical engineering from the University of Maryland, College Park, in 2003.



**Reza Ghodssi** (S'92–M'97) was born in Tehran, Iran, in 1966. He received the B.S., M.S., and Ph.D. degrees in electrical engineering from the University of Wisconsin at Madison in 1990, 1992 and 1996, respectively. His Ph.D. thesis was focused on development of a high aspect ratio microfabrication process for an electrostatic driven MEMS device using X-ray lithography and LIGA technology.

He was a Postdoctoral Associate and a Research Scientist in the Microsystems Technology Laboratories and the Gas Turbine Laboratory at the Massachusetts Institute of Technology (MIT) from 1997 to 1999. During his tenure at MIT, he developed the building block MEMS fabrication technologies for a microturbine generator device and also served as an Assistant Director on that project. In January 2000, he joined the Department of Electrical and Computer Engineering and the Institute for Systems Research at the University of Maryland (UMD), College Park, as an Assistant Professor. His research interests are in design and development of microfabrication technologies and their applications to microsensors, microactuators, and integrative microsystems.

Dr. Ghodssi received the 2001 UMD George Corcoran Award, 2002 National Science Foundation CAREER Award, and the 2003 UMD Outstanding Systems Engineering Faculty Award. He has served as a program co-chairman for the 2001 International Semiconductor Device Research Symposium (ISDRS) and since 2002 as a chairman of the MEMS and NEMS Technical Group at the American Vacuum Society (AVS). He is a co-founder of the MEMS Alliance Group in the greater Washington area and a member of the AVS and MRS.